ACS chemical biology

pubs.acs.org/acschemicalbiology

Articles

Merits of Diazirine Photo-Immobilization for Target Profiling of Natural Products and Cofactors

Polina Prokofeva, Stefanie Höfer, Maximilian Hornisch, Miriam Abele, Bernhard Kuster,* and Guillaume Médard*

Cite This: *ACS Chem. Biol.* 2022, 17, 3100–3109

Read Online

ACCESS | Metrics & More | Article Recommendations | Supporting Information

ABSTRACT: Finding the targets of natural products is of key importance in both chemical biology and drug discovery, and deconvolution of cofactor interactomes contributes to the functional annotation of the proteome. Identifying the proteins that underlie natural compound activity in phenotypic screens helps to validate the respective targets and, potentially, expand the druggable proteome. Here, we present a generally applicable protocol for the photoactivated immobilization of unmodified and microgram quantities of natural products on diazirine-decorated beads and their use for systematic affinity-based proteome profiling. We show that among 31 molecules of very diverse reported activity and biosynthetic origin, 25 could indeed be immobilized. Dose−response competition binding experiments using lysates of human or bacterial cells followed by quantitative mass spectrometry recapitulated targets of 9 molecules with <100 μM affinity. Among them, immobilization of coenzyme A produced a tool to interrogate proteins containing a HotDog domain. Surprisingly, immobilization of the cofactor flavin adenine dinucleotide (FAD) led to the identification of nanomolar interactions with dozens of RNA-binding proteins.

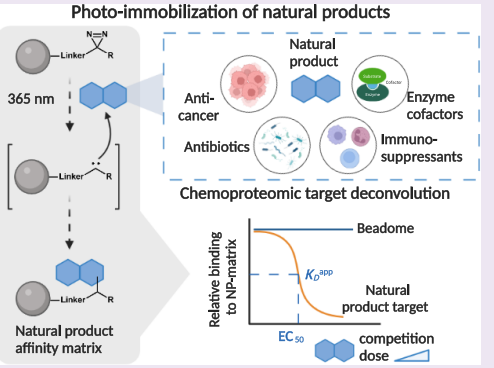

INTRODUCTION

In recent years, two major groups of mass spectrometry-coupled approaches have emerged as tools for target deconvolution of bioactive small molecules. "Label-free" techniques, which do not require modification of either protein or small molecule such as DARTS,[1] SPROX,[2] Lip-MS,[3] and CETSA[4]/TPP,[5] measure changes in biophysical properties of target proteins upon ligand binding. In contrast, methods such as AfBPP,[6] PAL,[7] and ABPP[8] rely on chemical probes that enrich protein targets from a biological source. Although label-free approaches are assumed to be rather unbiased, they suffer from the need to measure entire proteomes in order to find the often few individual proteins that change their physical properties within complex biological systems. While also laborious, the design and synthesis of chemical affinity probes offer an alternative that focuses on the analysis of a small part of the proteome that can be measured very efficiently. For naturally occurring molecules, the synthesis of appropriate probes is often prohibitive. Owing to their structural complexity, it can take years or even decades to complete the total synthesis of a natural compound or its derivatives. However, as an evolutionary enriched pool of biologically active compounds, natural products are a particularly interesting resource for chemical biology and drug discovery. The simple fact that they are produced by nature to serve a defined biological function provides sheer endless inspiration for drug design. From all small-molecule drugs approved between 1981 and 2019, 69% were either native natural products (NPs), derivatives thereof, or NP-inspired molecules.[9] Hence, NPs are frequently included in phenotypic drug screens, and many NPs with anticancer activities have been identified this way (e.g., paclitaxel).[10] High three-dimensional structure complexity and vast scaffold diversity, which make NPs so attractive for drug research, are also the major challenges for the synthesis of analogues, necessary for hit expansion and probe-based target deconvolution. In addition, given the often limited structure−activity relationships, rational installation of an enrichment handle that will not impair target binding may be difficult. Therefore, for a large number of bioactive natural products, targets and modes of action are still poorly understood.

To accelerate research of natural molecule action on the proteome, an expeditious general protocol for target deconvolution is highly desirable. To this end, Kanoh et al. pioneered the implementation of UV-induced photo-immobilization of small molecules. They repurposed the photoactivatable diazirine moiety, widely used for photoaffinity

Received: June 13, 2022
Accepted: October 5, 2022
Published: October 27, 2022

https://doi.org/10.1021/acschembio.2c00500
ACS Chem. Biol. 2022, 17, 3100−3109

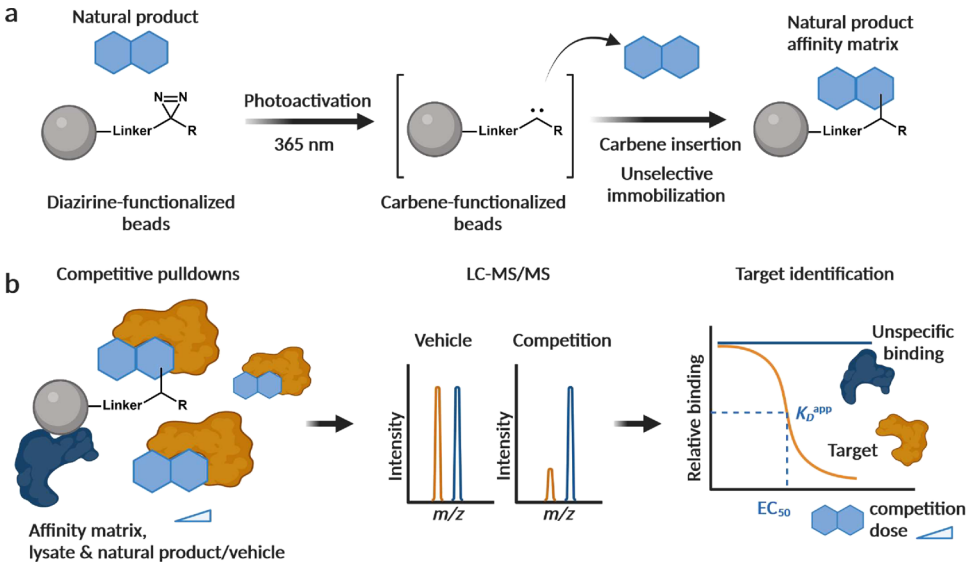

Figure 1. Workflow for target deconvolution using photo-immobilized affinity matrices. (a) Photo-crosslinking of natural products on diazirine-loaded beads through unselective carbene insertion. (b) Dose-dependent competition pulldown experiment of unmodified natural products and the corresponding affinity matrix coupled to quantitative mass spectrometry for protein identification and determination of apparent interaction constants (K_D^{app}); EC_{50}: effective concentration of natural product necessary to reduce protein binding to beads by 50%. Figure created with Biorender.com.

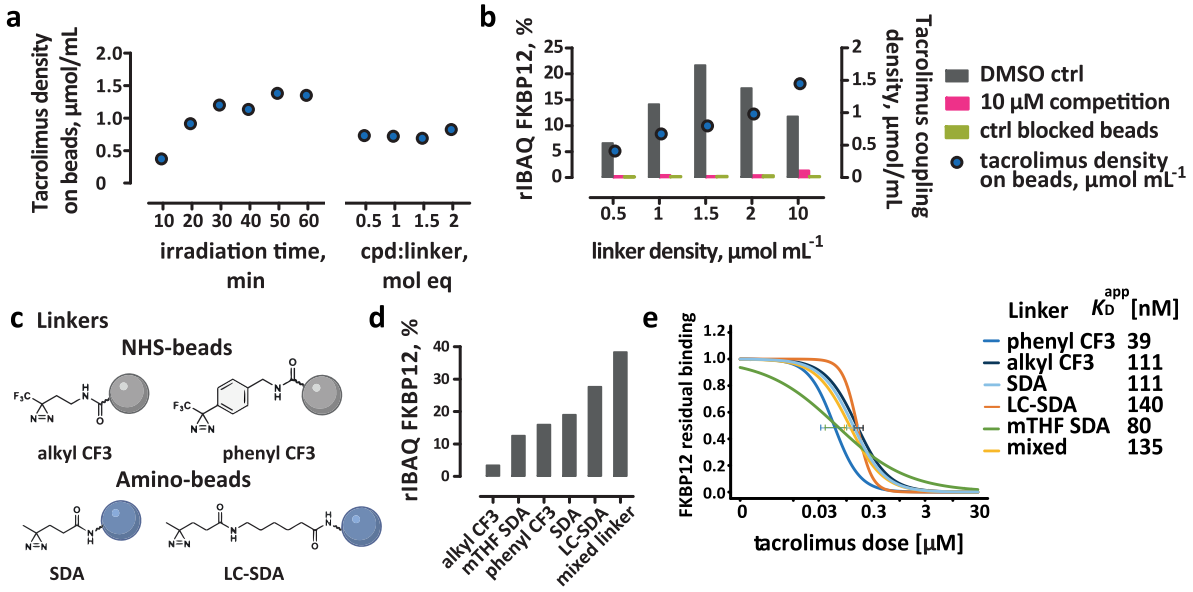

Figure 2. Optimization of photo-crosslinking conditions using tacrolimus as a model system. (a) Tacrolimus apparent loading on beads (blue circles) as a function of irradiation time or compound:linker ratio. 2 molar excess of tacrolimus was added to 2 μmol mL^{-1} LC-SDA-loaded beads for irradiation time tests; for cpd:linker optimization, a respective mol amount of tacrolimus was titrated to 2 μmol mL^{-1} LC-SDA-loaded beads. Tacrolimus final loading on beads was determined from LC−MS coupling controls (see Materials and Methods in the Supporting Information). (b) Relative amount of FKBP12 bound to beads (expressed as the fraction of FKBP12 vs total protein intensity-based absolute quantification, rIBAQ, %) as a function of linker density in the presence of DMSO (gray), in competition with 10 μM free tacrolimus (pink) and bound to beads that do not display immobilized tacrolimus (green, blocked beads). The blue circles indicate the density of tacrolimus on beads. (c) Structures of the diazirine linkers evaluated for photo-crosslinking of tacrolimus. (d) Relative amount of FKBP12 vs total protein bound to beads for the different linkers and the mixture of all linkers. (e) Residual binding of FKBP12 to beads as a function of increasing doses of free tacrolimus used as a competitor. Curve fitting was achieved using a four-parameter log-logistic regression model; the fit error is estimated with the error bars.

labeling (PAL) of protein targets, to photo-crosslinking of small molecules onto beads.[11] Upon UV irradiation, the diazirines that decorate the beads convert to carbenes and covalently insert (presumably randomly and promiscuously) into proximal C−H or X−H bonds of bead-adsorbed molecules (Figure 1a). The same group has also designed cleavable linkers that allow the release of the immobilized molecules to, for example, characterize the regioselectivity of such carbene insertions in different synthetic molecules and solvents.[12] They utilized this technology to immobilize the immunosuppressive drug of natural origin tacrolimus (FK506). A Novartis team recently adopted the approach to study chivosazole F, a natural product of unknown mode of action. By competition between immobilized chivosazole F and either

https://doi.org/10.1021/acschembio.2c00500
ACS Chem. Biol. 2022, 17, 3100−3109

a vehicle control (such as DMSO) or 100 μM chivosazole F dosed into a HEK293T cell lysate, they identified actin-containing protein complexes as interactors of chivosazole F.[13] A recent publication by Melder et al.[14] has shown that phenyl diazirine-decorated cellulose membranes can also be used for target screening of bioactive natural molecules. They have compared the protein enrichment by membranes loaded with cyclosporine A, tacrolimus, sirolimus, or lenalidomide with unmodified control membranes and recapitulated known binders of the drugs.[14] This approach adopts a different philosophy compared to more classical probe-based target deconvolution techniques: it bypasses the challenging synthesis of rationally designed analogues of the molecule of interest and embraces the promiscuity of carbene insertion chemistry. In this way, low quantities of unmodified molecules become amenable for target deconvolution. Inspired by this elegant concept, we sought to explore the scope and merits of unselective photo-immobilization using diazirine-functionalized beads for target profiling of natural compounds more systematically.

RESULTS AND DISCUSSION

Expeditious Workflow for Photo-Immobilization of Natural Products for Target Deconvolution. We first evaluated different parameters of the target deconvolution assay that capitalizes on established and robust protocols for affinity pulldown coupled to MS readout (Figure 1b).[15] Potent bioactive molecules are expected to show strong binding affinities for their protein targets. Therefore, an affinity matrix based on the chemical structure of the compound in question should efficiently enrich molecular targets from biological samples (lysates). In turn, these can then be identified agnostically using mass spectrometry. The main advantages of this assay are (1) a reduced proteome complexity, owing to the affinity enrichment step, which renders the MS readout more efficient, and (2) the affinity matrix that can be set to compete for target binding with the unmodified molecule of interest. When the assay is performed with a range of competitor concentrations in native lysate, it yields dose–response competition curves that characterize the binding across the panel of all enriched proteins and allows for target identification. The effective concentration of natural product necessary to reduce protein binding to beads by 50% (EC_{50}) can be determined from the curve and converted into an apparent interaction constant (K_D^{app}; see the Supporting Information for details). Manual inspection of all curves for all bead-bound proteins allows to *de novo* annotate proteins as targets of the analyzed natural molecules (Figure 1b).

To optimize UV-induced (365 nm) immobilization, we chose tacrolimus as a model compound. First, the optimal irradiation time was determined for beads loaded with 2 μmol mL^{-1} succinimidyl 6-(4,4′-azipentanamido)hexanoate (LC-SDA) and using a twofold molar excess of tacrolimus. We tested six irradiation times and observed that tacrolimus conversion reached a plateau after 30 min, which was used in all subsequent experiments (Figure 2a and Figure S1a). To assess the optimal compound-to-linker ratio, tacrolimus was titrated to the 2 μmol mL^{-1} LC-SDA beads in 0.5, 1.0, 1.5, and 2.0 molar equivalents. There was no obvious difference in tacrolimus loading to the beads within the tested range (Figure 2a and Figure S1b). Pulldowns using the above matrices and K562 cell lysate enriched FKBP12, the cognate target of tacrolimus, in comparable quantities (Figure S1d). Pulldowns in the presence of 10 μM tacrolimus as competitor confirmed the specificity of the enrichment with a slightly better performance for the affinity matrix prepared with equimolar amounts of linker and compound (Figure S1d). Usage of the equimolar compound-to-linker ratio was hence decided for all subsequent experiments. This turned out to be a good choice for the immobilization of all natural compounds tested in this study (Table S2).

With a fixed irradiation time (30 min) and compound-to-linker ratio (equimolar) in hand, we further evaluated the influence of the diazirine linker density on beads. As expected, immobilization on beads decorated with higher LC-SDA coupling densities led to higher absolute conversion (in mol amount) and higher apparent coupling density of tacrolimus (Figure 2b and Figure S1c). However, the reaction showed to be less and less efficient with increasing diazirine densities as a 20-times higher linker density was required to achieve a 3-fold higher coupling density of the compound (Figure S1c). The relative abundance of FKBP12 in pulldowns using these matrices ranged from 6% (vs 0.1% for control beads) to 20% (vs 0.2% for control beads) for beads prepared with 1.5 μmol ml^{-1} LC-SDA and tacrolimus (Figure 2b). At higher linker densities, we observed increased unspecific protein binding to beads, which led to lower relative FKBP12 abundance (Figure S2). Again, single-dose competition pulldown experiments using 10 μM tacrolimus for all affinity matrices also defined 1.5 μmol mL^{-1} as the optimum linker coupling density as the ratio of the amount of FKBP12 compared to vehicle was maximal (Figure 2b).

Obviously, the choice of photo-activatable linker is also important as its chemical nature can influence the efficiency of the carbene insertions. It has been shown that, upon UV irradiation, diazirines can undergo diazo-isomerization, resulting in undesired linear diazo-intermediates.[16] Length, bulkiness, or hydrophobicity of the spacer can also influence (un)desirable and (un)specific binding of proteins from cell lysates to beads. We, therefore, compared tacrolimus-loaded matrices prepared using four commercially available photo-activatable linkers. These are the LC-SDA linker discussed so far, a shorter version SDA and two trifluoromethyl diazirine molecules, namely, the alkyl CF_3 linker 2-(3-(trifluoromethyl)-3*H*-diazirin-3-yl)ethan-1-amine (CAS 2095409-03-1) and the analogous phenyl CF_3 linker (4-(3-(trifluoromethyl)-3*H*-diazirin-3-yl)phenyl)methanamine (CAS 1258874-29-1) (Figure 2c). Using the reaction conditions optimized above, tacrolimus conversion ranged between 25% (for LC-SDA) and 60% (for alkyl CF_3) (Table S2), and the CF_3 diazirine linkers were overall more efficient. But this did not translate into more efficient tacrolimus loading to beads or enrichment of FKBP12 (Table S2). The relative amounts of FKBP12 enriched on beads ranged from 3% for the most dense aliphatic trifluoromethyl-based beads to 27% for LC-SDA (Figure 2d). Since alkyl and aryl diazirines display different labeling preferences and that multiple functional groups can react with carbenes,[12,17] each carbene insertion is expected to follow its own regioselectivity rules for the different linkers. Moreover, the chains of atoms that separate the tacrolimus molecule from the bead surfaces may have a strong impact on the binding to FKBP12. As the immobilization approach relies on the unselective nature of carbene insertion, a (unknown) fraction of the immobilized compound may be inactive, leading to loss of protein binding. Another fraction might, however, be

https://doi.org/10.1021/acschembio.2c00500
ACS Chem. Biol. 2022, 17, 3100−3109

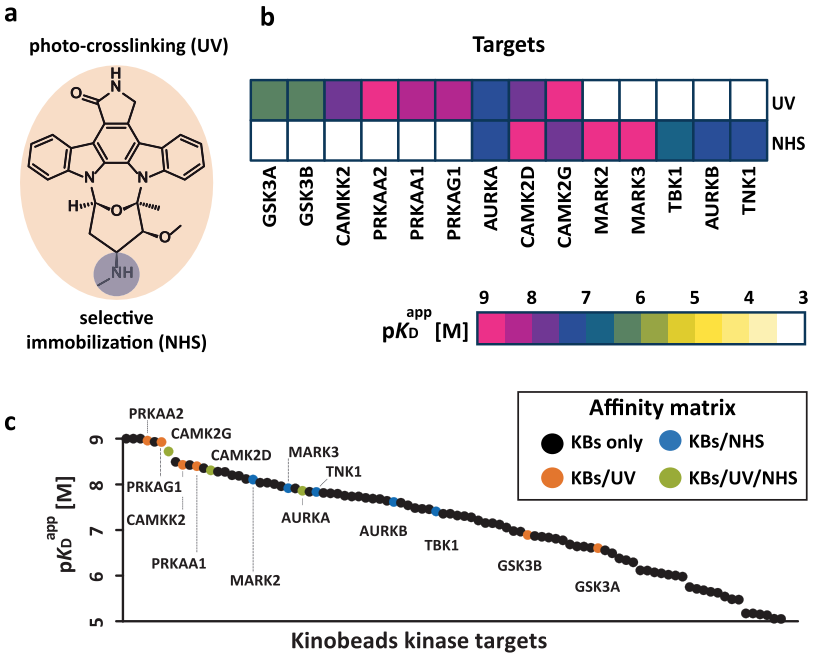

Figure 3. Comparison of target proteins identified by selective secondary amine vs photo-immobilization of staurosporine or Kinobeads. (a) Chemical structure of staurosporine with the secondary amine used for immobilization highlighted in blue (selective immobilization). The orange circle depicts that promiscuous UV-induced immobilization may occur anywhere in the compound. (b) Heatmap depicting apparent binding constants of protein targets obtained by photo-crosslinked or selectively immobilized staurosporine. (c) Apparent binding constants of all staurosporine kinase targets obtained by Kinobeads (KBs) profiling. The black dots indicate the targets that were only identified in Kinobeads assay, selectively immobilized staurosporine and Kinobeads (NHS, blue dots), UV-immobilized staurosporine and Kinobeads (orange), or by all three approaches (KBs, UV, and NHS, green dots).

attached via diverse anchor points that maintain bioactivity. Our experiments indicate that this balance is linker-dependent.

With the intention to generalize the experimental procedure, we performed pulldowns using a mixture of tacrolimus-functionalized beads that contain all four diazirine linkers. Here, FKBP12 constituted more than a third of the entire enriched sub-proteome (Figure 2d), and the dose−response curves for native FKBP12 obtained using individual linker-derived or mixed linker-based tacrolimus matrices were very similar and allowed the determination of consistent affinities (median 111 nM +/− 38 nM STD; Figure 2e and Table S1). Importantly, in these dose-dependent competition experiments with tacrolimus, among all bead-bound proteins, FKBP12 and this protein only showed the typical dose−response curve expected for a target. Clearly, would the target of tacrolimus be unknown, our assay would *de novo* deconvolute FKBP12 as the likely target of the drug (Table S3).

For all experiments so far, diazirine beads were evaporated to dryness, which alters beads' morphology and causes them to shrink. To compare affinity matrices produced in this way to immobilization in suspension, tacrolimus was added to SDA-loaded beads in radical-friendly mTHF and subjected to UV irradiation followed by a full dose competition pulldown using K562 cell lysate. Here, the enrichment of FKBP12 was reduced by more than a half (from 28 to 12% rFKBP12; Figure 2d) compared to dried beads, and the dose-dependent competition resulted in a poorer quality curve (Figure 2e). In light of the above, we fixed the assay conditions to 1.5 μmol mL^{-1} mixed diazirine-loaded beads and 1 molar equivalent of compound, which, following mixing, are evaporated to dryness and exposed to 30 min of UV irradiation at 365 nm (details of experimental procedures in the Supporting Information).

An important result of the optimization procedure thus far is that the novel multi-linker protocol requires less than 0.25 mg of compound to produce enough matrix for a full dose−response target deconvolution experiment. This is important as only very limited quantities of natural product can typically be isolated in practice.

Immobilization of Staurosporine via Carbene Insertion or Acylation Yield Complementary Target Profiles. Owing to the rich chemoproteomic history of staurosporine, we chose this natural broad kinase inhibitor to compare our multi-linker photo-immobilization method to conventional immobilization via acylation of the secondary amine (Figure 3a). A matrix obtained by the latter approach was included in the first version of Kinobeads, a kinome-enriching affinity matrix composed of seven linkable and broad-spectrum kinase inhibitors.[18] The Kinobeads approach identified 66 kinase targets with IC_{50} below 10 μM and 51 kinases that showed thermal shifts in the following CETSA-MS profiling. The authors also observed that about one-third of the kinase targets found by Kinobeads profiling did not show measurable thermal shifts upon binding.[19] We performed target deconvolution of (unmodified) staurosporine using full dose competition pulldowns against photo-crosslinked beads or against the compound coupled to NHS-activated beads (Figure 3b). Both matrices enriched a rather surprisingly small number of kinases, and only three targets were identified with similar affinities in both assays (AURKA, CAMK2D, and CAMK2G). Five kinases (AURKB, MARK2, MARK3, TBK1, and TNK1) were only found using NHS-immobilized staurosporine, and CAMKK2, GSK3A, GSK3B, PRKAA1, PRKAA2, and PRKAG1 were exclusively observed using photo-crosslinked beads. The two tailored affinity matrices

https://doi.org/10.1021/acschembio.2c00500
ACS Chem. Biol. 2022, 17, 3100−3109

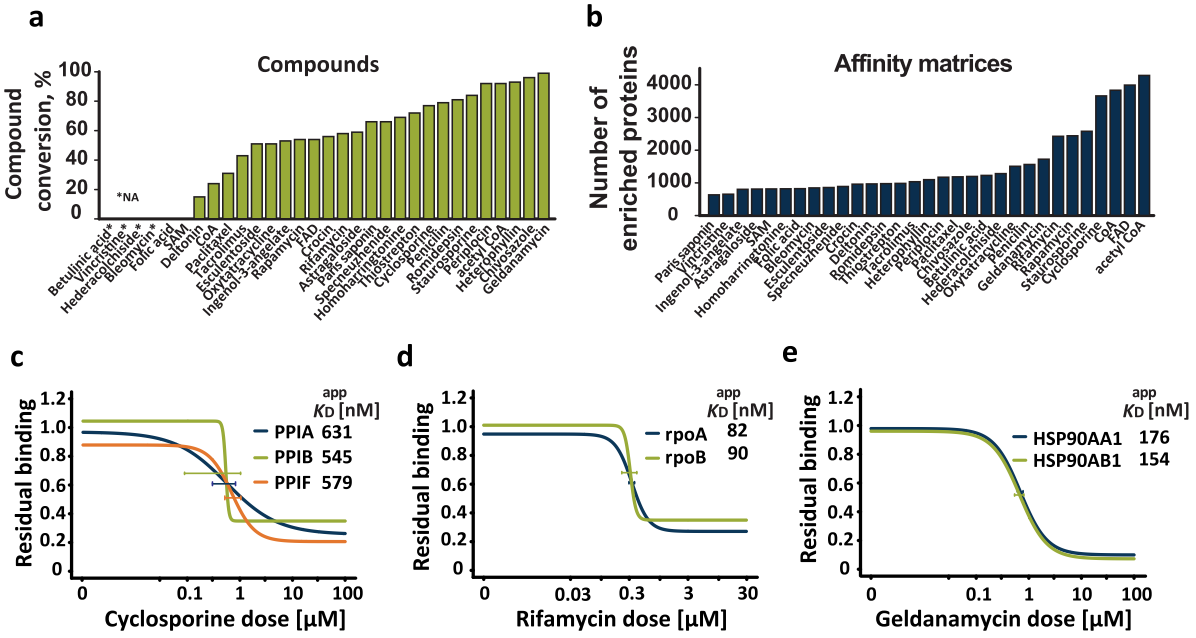

Figure 4. Broad assessment of photo-immobilization for target deconvolution of natural molecules. (a) Immobilization efficiency upon UV irradiation for 31 natural compounds. (b) Number of proteins bound by each affinity matrix. (c) Dose−response curves for cyclosporine A binders PPIA, PPIF, and PPIB. (d) Same as panel c but for rifamycin B. (e) Same as panel c but for geldanamycin.

also underperformed compared to the latest version of Kinobeads that do not contain immobilized staurosporine (Figure 3c).[20] Our Kinobeads profiling identified 94 kinase targets with affinities below 10 μM and included all the above targets. Based on the crystal structures of multiple staurosporine−kinase complexes, it is quite clear that immobilization of the molecule through its methylamino group can result in substantial changes in protein binding. For instance, acylation annihilates the often-observed hydrogen bond between the charged amine of the compound and ATP pocket residues of the kinase. As noted above, the carbene insertion reaction also affects the ability of the affinity matrix to engage targets, evidently, in a different way than the NHS-linked analogue(s) of staurosporine. Despite multiplying the chances of producing bioactive linked analogues by photo-crosslinking, the example of staurosporine highlights limitations of our approach in terms of how comprehensive it is with regard to target deconvolution.

Promiscuous Photo-Immobilization Enables Rapid Probing for Protein Binders of Natural Molecules. To evaluate the scope of our target deconvolution assay more broadly, we selected 31 commercially available natural molecules (including tacrolimus and staurosporine discussed above) of different biosynthetic origins. Among them are 3 common antibiotics, 5 cofactors of proteins, and 24 compounds with reported anticancer activity in at least one assay (Figure S3 and Table S2). After preparing their corresponding affinity matrices using our multi-linker protocol, we performed dose-dependent competition binding assays in human or bacterial cell lysates. Reassuringly, 25 of the 31 tested compounds (80%) could be immobilized with coupling efficiencies ranging between 15 and 99% (Figure 4a). Only two compounds failed to react with diazirine beads, while further four compounds do not possess a UV chromophore or did not generate the UV or MS signals necessary for quantifying their conversion by LC−MS. These measurements cannot conclude on the regioselectivity or potential cascading of the immobilization reaction, but they do indicate that the compounds are not excessively labile upon UV exposure, since side-products were not observed in the spectra. The number of proteins enriched by the 31 affinity matrices ranged from several hundreds to several thousands (Figure 4b). Protein binders have been described for about half of the compounds, and we were able to recapitulate known targets for eight compounds (Table S2). For compounds without described protein binders, our assay also did not uncover any. There may be many reasons for not capturing targets in addition to the ones outlined above. For instance, the protein may not be expressed in the cells we used here, they may not retain their natural fold under the conditions of lysis, or the interaction may be too transient to capture. Some NPs may be prodrugs that may be inactive in lysates, while others may not bind proteins as their normal mode of action. Bleomycin, for example, covalently binds to nucleic acids and catalyzes their oxidation, which, in turn, is leading to scission of DNA and cell death. Six of the 31 compounds tested here are saponins. These form complexes with cholesterol and create pores in the cell membrane to kill cells. Such compounds would not be expected to score in our assay because of their particular mode of action. Despite the seemingly low overall success rate, we point out that none of the alternatives such as the aforementioned DARTS,[1] SPROX,[2] Lip-MS,[3] CETSA[4]/TPP,[5] AfBPP,[6] PAL,[7] or ABPP[8] is universal either. At the same time, our approach is technically very straightforward, alleviates extensive probe synthesis while being thrifty in measurement time, and can be deployed to a wide range of biological systems so that it is certainly worth considering for target deconvolution, as illustrated below.

Among the successful cases, we recapitulated known binders of the immunosuppressant cyclosporine A, including the cyclophilins PPIA (K_D^{app} 631 nM), PPIB (K_D^{app} 545 nM), and PPIF (K_D^{app} 579 nM)[21] in human cells (Figure 4c). Similarly, we found targets of the macrocyclic polyketide antibiotics rifamycin B (Figure 4d) and geldanamycin (Figure

https://doi.org/10.1021/acschembio.2c00500
ACS Chem. Biol. 2022, 17, 3100−3109

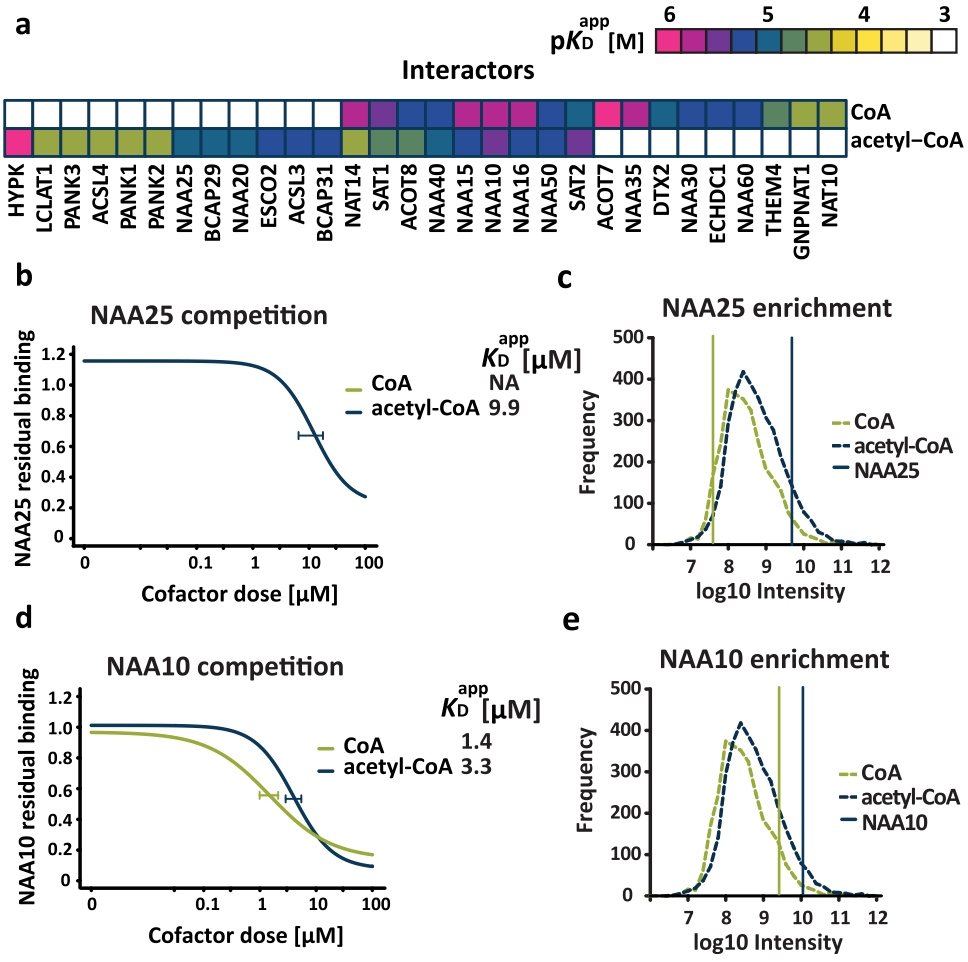

Figure 5. Binders of the protein cofactors CoA and acetyl-CoA. (a) Heatmap of apparent interaction constants of protein binders of CoA and acetyl-CoA. (b) Residual binding of NAA25 to CoA and acetyl-CoA beads in response to increasing concentrations of free CoA and acetyl-CoA, respectively. (c) Intensity distribution of all proteins bound to CoA or acetyl-CoA beads (dotted lines). The solid lines mark the position of NAA25 in these distributions. (d) Same as panel b but for NAA10. (e) Same as panel c but for NAA10.

4e) in bacterial *Escherichia coli* and human colorectal cancer SW-620 lysates, respectively.[22−24] For rifamycin B, its cognate target, DNA-directed RNA polymerase subunit beta (rpoB) was identified (K_D^{app} 90 nM) along with the subunit alpha (rpoA), likely as a result of co-enrichment and co-competition (Figure 4d). Geldanamycin is a heat-shock protein 90 (HSP90) inhibitor, and competition pulldowns identified two HSP90s as geldanamycin targets (HSP90AA1, K_D^{app} 176 nM; HSP90AB1, K_D^{app} 154 nM; Figure 4e). Together, these results indicate that photo-crosslinking immobilization deserves consideration in future antibiotics discovery because it is easily deployable in human and bacterial lysates and could, therefore, help uncover targets of novel antibiotics based on natural compounds.

CoA and Acetyl-CoA Interact with Multiple Acyltransferases and HotDog Domain Proteins. Besides target deconvolution for drug discovery, another interesting application of our approach is the delineation of interactors of protein cofactors. Such objective has been the focus of inspiring publications, in which cofactor analogues, for example, NAD and acyl-CoA, have been synthesized as affinity probes to explore interactomes.[25,26] For instance, Levy et al. created a lysine-CoA matrix to investigate the specificity of protein binders to different acyl-CoAs.[27] More specifically, a Lys-CoA probe was set to compete with multiple CoA metabolites at 30 μM dose, which led to the identification of 166 proteins that showed at least twofold reduction of binding to free coenzyme A. From those, 126 proteins were also found using photo-immobilized CoA in this study. However, only seven of these proteins displayed a clear dose−response curve, unequivocally identifying as CoA binders with affinities below 100 μM (Table S3).

We have further immobilized acetyl-CoA using our method in order to compare its binding profile to the one of CoA. The two photo-immobilized cofactors shared 9 protein binders among the total of 30 competed proteins with affinities below 100 μM (Figure 5a). As one might expect, many of the found binders are known acyl-CoA interactors such as the acyltransferases NAT14, NAA25, NAA20, NAA30, NAA40, NAA15, NAA10, NAA16, NAA50, SAT1, and SAT2. Among those, several acyltransferases showed selective binding to one of the cofactors. For example, NAA25 showed typical dose-dependent intensity reduction exclusively in competition with acetyl-CoA, whereas the CoA matrix failed to stably enrich it from SW-620 cell lysate (Figure 5b,c). Conversely, multiple acyltransferases were bound and competed by both molecules, for example, NAA10 (Figure 5d,e).

Another group of specific binders contain a HotDog domain (THEM4, ACOT13, ACOT7, ACOT8, ACOT9, HSD17B4, and THEM6), found in several human thioesterases, which

https://doi.org/10.1021/acschembio.2c00500
ACS Chem. Biol. 2022, 17, 3100−3109

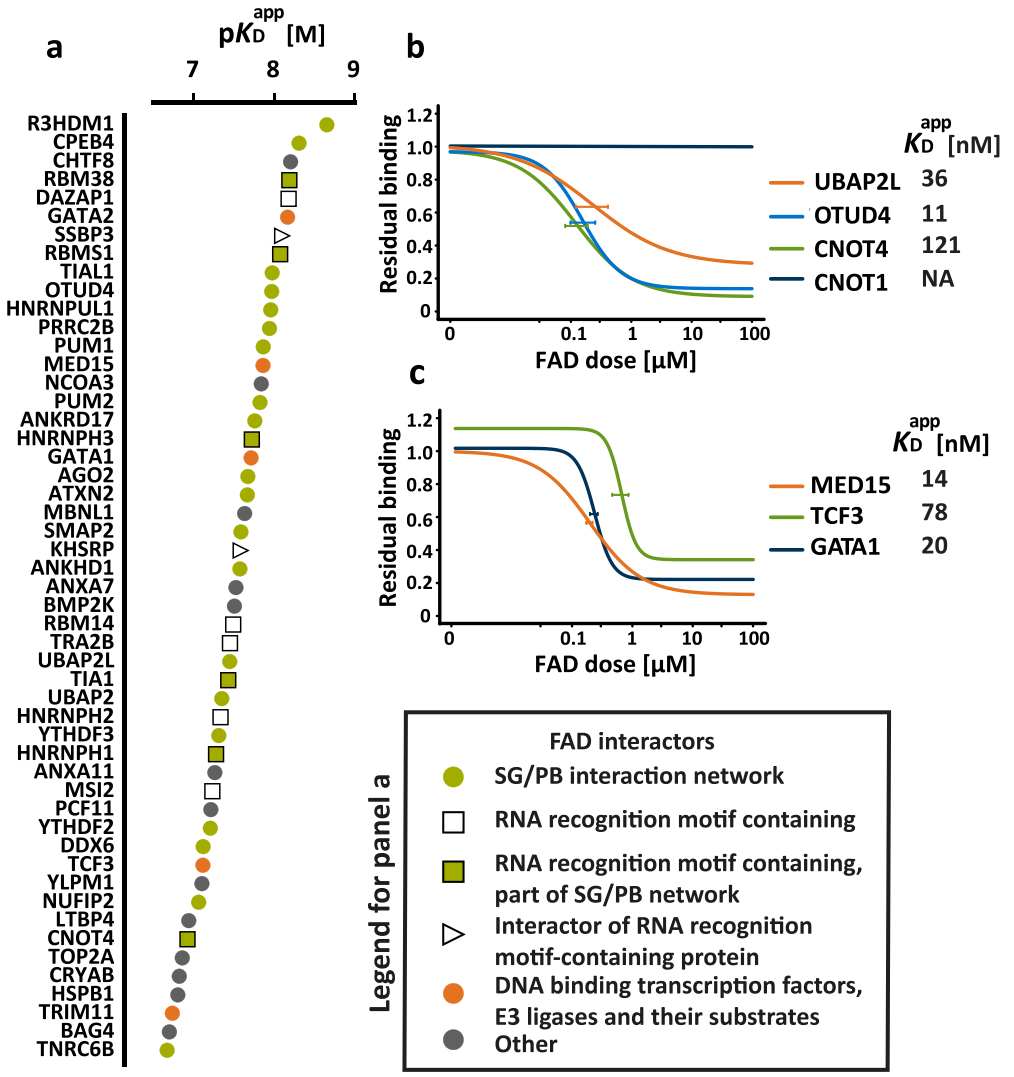

Figure 6. FAD interactors. (a) Affinity ranking of all identified direct or indirect FAD interactors in a full dose competition pulldown assay. (b) Dose−response curves for identified FAD binders UBAP2L, OTUD4, and CNOT4. CNOT1 was bound by the matrix but not competed up to 100 μM. (c) Same as panel b but for MED15, TCF3, and GATA1.

links them to acetyl-CoA biochemistry. Overall, of the 12 human HotDog domain-containing proteins reviewed by UniProt, seven and five were enriched by the coenzyme A and acetyl-CoA matrices, respectively. We also observed competition of HotDog domain-containing THEM4 and ACOT7 by coenzyme A. THEM4/CTMP has been reported as an oncogene in breast cancer, while ACOT7 appears to play an important role in inflammatory disease and breast and lung cancer development.[28−30] The easily obtained matrices could hence be suitable to profile potential inhibitors of these enzymes.

The Cofactor Flavin Adenine Dinucleotide (FAD) Is a Nanomolar Binder of RNA-Binding Proteins. As a third example, we explored the interactome of flavin adenine dinucleotide (FAD) and the matrix of UV-immobilized FAD bound more than 3000 proteins from SW-620 lysate. Among these were 17 known FAD-binding flavoproteins[31] (GCDH, ACADVL, KDM1A, ETFDH, ETFA, SDHA, PPOX, CYB5R1, SQLE, POR, CYB5R3, AIFM1, ACOX1, ILVBL, AGPS, ACOX3, and DLD), but none was competed by free FAD. Flavoenzymes use flavins as prosthetic groups and are known to bind the flavin cofactor very tightly, some even covalently as part of the holoenzyme.[32] Particularly, the covalent binders would not be expected to bind an FAD matrix at all and may indicate that the 17 proteins mentioned above are likely poor binders of FAD with affinities weaker than our higher dose.

GO enrichment analysis showed that about 600 RNA-binding proteins were bound to FAD beads (Figure S4) and, surprisingly, more than 40 proteins showed clear dose-dependent binding competition with nanomolar affinities, indicating that their direct or indirect interaction with free FAD is both specific and strong (Figure 6). Some insight into these unexpected interactions comes from a BioID profiling study of mRNA-associated stress granules (SGs) by Youn et al.[33] This published high-confidence proximity interaction network includes key regulators of SG formation (OTUD4, UBAP2L, CSDE1, and PRRC2C; Figure 6) or proteins recruited to SGs in response to stress (G3BP1, PABPC1, and eIF4A1). While all seven proteins were identified on FAD beads, only the ubiquitin-associated protein 2-like protein UBAP2L and the deubiquitinase OTUD4 showed potent competition with free FAD (K_D^{app} 36 and 11 nM, respectively; Figure 6a,b).

https://doi.org/10.1021/acschembio.2c00500
ACS Chem. Biol. 2022, 17, 3100−3109

Another noteworthy example is the CCR4−NOT deadenylase complex. Of the five detected CNOT proteins (CNOT1−4 and CNOT10), only the E3 ubiquitin ligase CNOT4 was competed (K_D^{app} 121 nM; Figure 6b). Known direct interactors of the complex such as the GW182 protein TNRC6B (K_D^{app} 217 nM) and the endonuclease Argonaute AGO2 (K_D^{app} 21 nM) were also competed,[34] along with CNOT BioID proximity interactors reported by Youn et al.[33] (Figure 6a). We note that several of these proteins contain canonical RNA-binding domains, such as RRM, PUM-HD, or KH domains, or are known to be involved in mRNA metabolism or regulation of transcription (HNRNPH1, 53 nM; HNRNPH2, 47 nM; HNRNPH3, 19 nM; HNRNPUL1, 11 nM; MBNL1, 23 nM; CPEB4, 5 nM; PUM1, 14 nM; ANKHD1, 27 nM).[35−37] Yet, others have seemingly unrelated annotated functions (ATXN2, 22 nM; ANKRD17, 18 nM). Several further proteins are rather poorly functionally annotated (R3HDM1, 2 nM; SMAP2, 26 nM; PRRC2B, 12 nM), but the results obtained here may also place them into the functional context of mRNA metabolism, SG formation, or regulation of transcription.

The DNA-binding transcription factors GATA1, GATA2, and TCF3 and a member of the mediator complex MED15 also showed potent direct or indirect FAD binding (K_D^{app} 20, 7, 78, and 14 nM, respectively; Figure 6c) as well as the E3 ligase TRIM11 (K_D^{app} 186 nM). It has been shown that TRIM11 negatively regulates MED15 stability and reduces its transcriptional activity that, again, links FAD to ubiquitin-regulated cellular processes.

Among the few known consensus sequences for RNA-binding proteins, we selected the PUF motif 5′-UGUANAUA-3′ to investigate whether FAD is binding the Pumilio homologues PUM1 and PUM2 in their RNA-binding pocket, as both these proteins showed dose−response behavior in the FAD versus FAD beads (Figure 6a).[38,39] Immobilization of an oligomer containing the consensus sequence on NHS-activated Sepharose beads yielded PUM beads that did enrich the Pumilio homologues (Figure S5a−c). Oligomer vs FAD beads and FAD vs PUM beads together with the FAD vs FAD beads dose−response competition indicated that the binding of FAD does not seem to influence the binding of the RNA (Figure S5d,e). It is therefore most likely that FAD binding is allosteric for PUMs.

An important future line of research in this context is to further explore the mechanism of FAD binding and show which of the discussed proteins are direct binders, to which part of the FAD molecule the proteins bind, and how such binding may be involved in regulating processes such as mRNA deadenylation or DNA binding.

CONCLUSIONS

In conclusion, the current work for the first time broadly evaluated the combination of diazirine photo-immobilization and proteomics for target deconvolution of natural molecules. We proposed an experimentally straightforward approach for the preparation of tailored affinity matrices using mixed diazirine beads, combined with dose-dependent competition assay and mass spectrometry readout. The versatile workflow was applied to a wide range of natural compounds and protein cofactors. Even though the overall success rate is moderate and highly dependent on the natural molecule in question, we propose that the simplicity and generality of the experimental procedure as well as the very quantitative characteristic of the proteomic readout may make it the first "go-to method" to probe natural molecules for protein binding. The latter is underscored by the surprising finding that UV-immobilized FAD led to the discovery of nanomolar protein−FAD interactions including multiple members of the ubiquitin system. This follows earlier unexpected observations made for immobilized kinase inhibitors that identified the clinically relevant off-target ferrochelatase (FECH)[40] or the identification of low nanomolar interactions and inhibition of the protein MBLAC2 by HDAC inhibitors.[41] By extending the chemical proteomic approach presented here to further natural molecules, it can be anticipated that more such surprising interactions will be uncovered, which, in turn, will improve our understanding of the cellular phenotypes elicited by such molecules as well as their cellular mode of action.

Present Addresses. Maximilian Hornisch—Max Delbrück Center for Molecular Medicine in the Helmholtz Association (MDC), 13125 Berlin, Germany.

ASSOCIATED CONTENT

Data Availability Statement

Data tables, data plotting, raw MS files, and MaxQuant searches are available for download on ProteomeXchange PRIDE repository under the identifiers PXD033292 and PXD036953.

Supporting Information

The Supporting Information is available free of charge at https://pubs.acs.org/doi/10.1021/acschembio.2c00500.

Detailed experimental procedures (bead preparation, compound conversion calculation from coupling controls, pulldown assay, cell culture, and data analysis), as well as additional details on data availability, assay optimization, and profiling results (PDF)

AUTHOR INFORMATION

Corresponding Authors

Bernhard Kuster − *Chair of Proteomics and Bioanalytics, TUM School of Life Sciences and Bavarian Center for Biomolecular Mass Spectrometry (BayBioMS), Technical University of Munich, 85354 Freising, Germany;* orcid.org/0000-0002-9094-1677; Email: kuster@tum.de

Guillaume Médard − *Chair of Proteomics and Bioanalytics, TUM School of Life Sciences, Technical University of Munich, 85354 Freising, Germany;* orcid.org/0000-0002-4782-4029; Email: g.medard@tum.de

Authors

Polina Prokofeva − *Chair of Proteomics and Bioanalytics, TUM School of Life Sciences, Technical University of Munich, 85354 Freising, Germany*

Stefanie Höfer − *Chair of Proteomics and Bioanalytics, TUM School of Life Sciences, Technical University of Munich, 85354 Freising, Germany*

Maximilian Hornisch − *Chair of Proteomics and Bioanalytics, TUM School of Life Sciences, Technical University of Munich, 85354 Freising, Germany*

Miriam Abele − *Chair of Proteomics and Bioanalytics, TUM School of Life Sciences and Bavarian Center for Biomolecular Mass Spectrometry (BayBioMS), Technical University of Munich, 85354 Freising, Germany*

Complete contact information is available at: https://pubs.acs.org/10.1021/acschembio.2c00500

Author Contributions

The manuscript was written through contributions of all authors. All authors have given approval to the final version of the manuscript.

Notes

The authors declare no competing financial interest.

■ ACKNOWLEDGMENTS

We gratefully acknowledge funding by the Deutsche Forschungsgemeinschaft (DFG, project 452256511). M.A. was supported by the EU Horizon 2020 grant Epic-XS.

■ REFERENCES

(1) Lomenick, B.; Hao, R.; Jonai, N.; Chin, R. M.; Aghajan, M.; Warburton, S.; Wang, J.; Wu, R. P.; Gomez, F.; Loo, J. A.; Wohlschlegel, J. A.; Vondriska, T. M.; Pelletier, J.; Herschman, H. R.; Clardy, J.; Clarke, C. F.; Huang, J. Target Identification Using Drug Affinity Responsive Target Stability (DARTS). *Proc. Natl. Acad. Sci. U. S. A.* **2009**, *106*, 21984−21989.

(2) West, G. M.; Tang, L.; Fitzgerald, M. C. Thermodynamic Analysis of Protein Stability and Ligand Binding Using a Chemical Modification- and Mass Spectrometry-Based Strategy. *Anal. Chem.* **2008**, *80*, 4175−4185.

(3) Feng, Y.; De Franceschi, G.; Kahraman, A.; Soste, M.; Melnik, A.; Boersema, P. J.; De Laureto, P. P.; Nikolaev, Y.; Oliveira, A. P.; Picotti, P. Global Analysis of Protein Structural Changes in Complex Proteomes. *Nat. Biotechnol.* **2014**, *32*, 1036−1044.

(4) Martinez Molina, D.; Nordlund, P. The Cellular Thermal Shift Assay: A Novel Biophysical Assay for in Situ Drug Target Engagement and Mechanistic Biomarker Studies. *Annu. Rev. Pharmacol. Toxicol.* **2016**, *56*, 141−161.

(5) Franken, H.; Mathieson, T.; Childs, D.; Sweetman, G. M. A.; Werner, T.; Tögel, I.; Doce, C.; Gade, S.; Bantscheff, M.; Drewes, G.; Reinhard, F. B. M.; Huber, W.; Savitski, M. M. Thermal Proteome Profiling for Unbiased Identification of Direct and Indirect Drug Targets Using Multiplexed Quantitative Mass Spectrometry. *Nat. Protoc.* **2015**, *10*, 1567−1593.

(6) Schirle, M.; Bantscheff, M.; Kuster, B. Mass Spectrometry-Based Proteomics in Preclinical Drug Discovery. *Chem. Biol.* **2012**, *19*, 72−84.

(7) Murale, D. P.; Hong, S. C.; Haque, M. M.; Lee, J. S. Photo-Affinity Labeling (PAL) in Chemical Proteomics: A Handy Tool to Investigate Protein-Protein Interactions (PPIs). *Proteome Science*. BioMed Central Ltd. June 24, **2017**.

(8) Cravatt, B. F.; Wright, A. T.; Kozarich, J. W. Activity-Based Protein Profiling: From Enzyme Chemistry to Proteomic Chemistry. *Annu. Rev. Biochem.* **2008**, *77*, 383−414.

(9) Newman, D. J.; Cragg, G. M. Natural Products as Sources of New Drugs over the Nearly Four Decades from 01/1981 to 09/2019. *J. Nat. Prod.* **2020**, *83*, 770−803.

(10) Wani, M. C.; Horwitz, S. B. Nature as a Remarkable Chemist: A Personal Story of the Discovery and Development of Taxol. *Anti-Cancer Drugs* **2014**, *25*, 482−487.

(11) Kanoh, N.; Honda, K.; Simizu, S.; Muroi, M.; Osada, H. Photo-Cross-Linked Small-Molecule Affinity Matrix for Facilitating Forward and Reverse Chemical Genetics. *Angew. Chem.* **2005**, *44*, 3559−3562.

(12) Suzuki, T.; Okamura, T.; Tomohiro, T.; Iwabuchi, Y.; Kanoh, N. Third Generation Photo-Cross-Linked Small-Molecule Affinity Matrix: A Photoactivatable and Photocleavable System Enabling Quantitative Analysis of the Photo-Cross-Linked Small Molecules and Their Target Purification. *Bioconjugate Chem.* **2015**, *26*, 389−395.

(13) Filipuzzi, I.; Thomas, J. R.; Pries, V.; Estoppey, D.; Salcius, M.; Studer, C.; Schirle, M.; Hoepfner, D. Direct Interaction of Chivosazole F with Actin Elicits Cell Responses Similar to Latrunculin A but Distinct from Chondramide. *ACS Chem. Biol.* **2017**, *12*, 2264−2269.

(14) Melder, F. T.; Lindemann, P.; Welle, A.; Trouillet, V.; Heißler, S.; Nazaré, M.; Selbach, M.Compound Interaction Screen on a Photoactivatable Cellulose Membrane (CISCM) Identifies Drug Targets. *ChemMedChem* 2022, DOI: 10.1002/cmdc.202200346.

(15) Médard, G.; Pachl, F.; Ruprecht, B.; Klaeger, S.; Heinzlmeir, S.; Helm, D.; Qiao, H.; Ku, X.; Wilhelm, M.; Kuehne, T.; Wu, Z.; Dittmann, A.; Hopf, C.; Kramer, K.; Kuster, B. Optimized Chemical Proteomics Assay for Kinase Inhibitor Profiling. *J. Proteome Res.* **2015**, *14*, 1574−1586.

(16) Das, J. Aliphatic Diazirines as Photoaffinity Probes for Proteins: Recent Developments. *Chem. Rev.* **2011**, *111*, 4405−4417.

(17) West, A. V.; Muncipinto, G.; Wu, H. Y.; Huang, A. C.; Labenski, M. T.; Jones, L. H.; Woo, C. M. Labeling Preferences of Diazirines with Protein Biomolecules. *J. Am. Chem. Soc.* **2021**, *143*, 6691−6700.

(18) Bantscheff, M.; Eberhard, D.; Abraham, Y.; Bastuck, S.; Boesche, M.; Hobson, S.; Mathieson, T.; Perrin, J.; Raida, M.; Rau, C.; Reader, V.; Sweetman, G.; Bauer, A.; Bouwmeester, T.; Hopf, C.; Kruse, U.; Neubauer, G.; Ramsden, N.; Rick, J.; Kuster, B.; Drewes, G. Quantitative Chemical Proteomics Reveals Mechanisms of Action of Clinical ABL Kinase Inhibitors. *Nat. Biotechnol.* **2007**, *25*, 1035−1044.

(19) Savitski, M. M.; Reinhard, F. B. M.; Franken, H.; Werner, T.; Savitski, M. F.; Eberhard, D.; Molina, D. M.; Jafari, R.; Dovega, R. B.; Klaeger, S.; Kuster, B.; Nordlund, P.; Bantscheff, M.; Drewes, G. Tracking Cancer Drugs in Living Cells by Thermal Profiling of the Proteome. *Science* **2014**, *346*, 1255784.

(20) Reinecke, M.; Ruprecht, B.; Poser, S.; Wiechmann, S.; Wilhelm, M.; Heinzlmeir, S.; Kuster, B.; Médard, G. Chemoproteomic Selectivity Profiling of PIKK and PI3K Kinase Inhibitors. *ACS Chem. Biol.* **2019**, *14*, 655−664.

(21) Davis, T. L.; Walker, J. R.; Campagna-Slater, V.; Finerty, P. J.; Finerty, P. J.; Paramanathan, R.; Bernstein, G.; Mackenzie, F.; Tempel, W.; Ouyang, H.; Lee, W. H.; Eisenmesser, E. Z.; Dhe-Paganon, S. Structural and Biochemical Characterization of the Human Cyclophilin Family of Peptidyl-Prolyl Isomerases. *PLoS Biol.* **2010**, *8*, No. e1000439.

(22) Floss, H. G.; Yu, T. W. Rifamycin - Mode of Action, Resistance, and Biosynthesis. *Chem. Rev.* **2005**, *105*, 621−632.

(23) Campbell, E. A.; Korzheva, N.; Mustaev, A.; Murakami, K.; Nair, S.; Goldfarb, A.; Darst, S. A. Structural Mechanism for Rifampicin Inhibition of Bacterial RNA Polymerase. *Cell* **2001**, *104*, 901−912.

(24) Roe, S. M.; Prodromou, C.; O'Brien, R.; Ladbury, J. E.; Piper, P. W.; Pearl, L. H. Structural Basis for Inhibition of the Hsp90 Molecular Chaperone by the Antitumor Antibiotics Radicicol and Geldanamycin. *J. Med. Chem.* **1999**, *42*, 260−266.

(25) Šileikytė, J.; Sundalam, S.; David, L. L.; Cohen, M. S. Chemical Proteomics Approach for Profiling the NAD Interactome. *J. Am. Chem. Soc.* **2021**, *143*, 6787−6791.

(26) Montgomery, D. C.; Garlick, J. M.; Kulkarni, R. A.; Kennedy, S.; Allali-Hassani, A.; Kuo, Y. M.; Andrews, A. J.; Wu, H.; Vedadi, M.; Meier, J. L. Global Profiling of Acetyltransferase Feedback Regulation. *J. Am. Chem. Soc.* **2016**, *138*, 6388−6391.

(27) Levy, M. J.; Montgomery, D. C.; Sardiu, M. E.; Montano, J. L.; Bergholtz, S. E.; Nance, K. D.; Thorpe, A. L.; Fox, S. D.; Lin, Q.; Andresson, T.; Florens, L.; Washburn, M. P.; Meier, J. L. A Systems Chemoproteomic Analysis of Acyl-CoA/Protein Interaction Networks. *Cell Chem. Biol.* **2020**, *27*, 322−333.e5.

(28) Liu, Y. P.; Liao, W. C.; Ger, L. P.; Chen, J. C.; Hsu, T. I.; Lee, Y. C.; Chang, H. T.; Chen, Y. C.; Jan, Y. H.; Lee, K. H.; Zeng, Y. H.; Hsiao, M.; Lu, P. J. Carboxyl-Terminal Modulator Protein Positively Regulates Akt Phosphorylation and Acts as an Oncogenic Driver in Breast Cancer. *Cancer Res.* **2013**, *73*, 6194−6205.

(29) Forwood, J. K.; Thakur, A. S.; Guncar, G.; Marfori, M.; Mouradov, D.; Meng, W.; Robinson, J.; Huber, T.; Kellie, S.; Martin, J. L.; Hume, D. A.; Kobe, B. Structural Basis for Recruitment of Tandem Hotdog Domains in Acyl-CoA Thioesterase 7 and Its Role in Inflammation. *Proc. Natl. Acad. Sci. U. S. A.* **2007**, *104*, 10382−10387.

(30) Jung, S. H.; Lee, H. C.; Hwang, H. J.; Park, H. A.; Moon, Y. A.; Kim, B. C.; Lee, H. M.; Kim, K. P.; Kim, Y. N.; Lee, B. L.; Lee, J. C.; Ko, Y. G.; Park, H. J.; Lee, J. S. Acyl-CoA Thioesterase 7 Is Involved in Cell Cycle Progression via Regulation of PKCζ-P53-P21 Signaling Pathway. *Cell Death Dis.* **2017**, *8*, No. e2793.
(31) Lienhart, W. D.; Gudipati, V.; MacHeroux, P. The Human Flavoproteome. *Arch. Biochem. Biophys.* **2013**, *535*, 150−162.
(32) Hefti, M. H.; Vervoort, J.; Van Berkel, W. J. H. Deflavination and Reconstitution of Flavoproteins: Tackling Fold and Function. *Eur. J. Biochem.* **2003**, *270*, 4227−4242.
(33) Youn, J. Y.; Dunham, W. H.; Hong, S. J.; Knight, J. D. R.; Bashkurov, M.; Chen, G. I.; Bagci, H.; Rathod, B.; MacLeod, G.; Eng, S. W. M.; Angers, S.; Morris, Q.; Fabian, M.; Côté, J. F.; Gingras, A. C. High-Density Proximity Mapping Reveals the Subcellular Organization of MRNA-Associated Granules and Bodies. *Mol. Cell* **2018**, *69*, 517−532.e11.
(34) Shirai, Y. T.; Suzuki, T.; Morita, M.; Takahashi, A.; Yamamoto, T. Multifunctional Roles of the Mammalian CCR4-NOT Complex in Physiological Phenomena. *Front. Genet.* **2014**, *5*, 1−11.
(35) Hegele, A.; Kamburov, A.; Grossmann, A.; Sourlis, C.; Wowro, S.; Weimann, M.; Will, C. L.; Pena, V.; Lührmann, R.; Stelzl, U. Dynamic Protein-Protein Interaction Wiring of the Human Spliceosome. *Mol. Cell* **2012**, *45*, 567−580.
(36) Wan, C.; Borgeson, B.; Phanse, S.; Tu, F.; Drew, K.; Clark, G.; Xiong, X.; Kagan, O.; Kwan, J.; Bezginov, A.; Chessman, K.; Pal, S.; Cromar, G.; Papoulas, O.; Ni, Z.; Boutz, D. R.; Stoilova, S.; Havugimana, P. C.; Guo, X.; Malty, R. H.; Sarov, M.; Greenblatt, J.; Babu, M.; Derry, W. B.; Tillier, E. R.; Wallingford, J. B.; Parkinson, J.; Marcotte, E. M.; Emili, A. Panorama of Ancient Metazoan Macromolecular Complexes. *Nature* **2015**, *525*, 339−344.
(37) Paul, S.; Dansithong, W.; Jog, S. P.; Holt, I.; Mittal, S.; Brook, J. D.; Morris, G. E.; Comai, L.; Reddy, S. Expanded CUG Repeats Dysregulate RNA Splicing by Altering the Stoichiometry of the Muscleblind 1 Complex. *J. Biol. Chem.* **2011**, *286*, 38427−38438.
(38) Afroz, T.; Skrisovska, L.; Belloc, E.; Guillén-Boixet, J.; Méndez, R.; Allain, F. H. T. A Fly Trap Mechanism Provides Sequence-Specific RNA Recognition by CPEB Proteins. *Genes Dev.* **2014**, *28*, 1498−1514.
(39) Van Nostrand, E. L.; Freese, P.; Pratt, G. A.; Wang, X.; Wei, X.; Xiao, R.; Blue, S. M.; Chen, J. Y.; Cody, N. A. L.; Dominguez, D.; Olson, S.; Sundararaman, B.; Zhan, L.; Bazile, C.; Bouvrette, L. P. B.; Bergalet, J.; Duff, M. O.; Garcia, K. E.; Gelboin-Burkhart, C.; Hochman, M.; Lambert, N. J.; Li, H.; McGurk, M. P.; Nguyen, T. B.; Palden, T.; Rabano, I.; Sathe, S.; Stanton, R.; Su, A.; Wang, R.; Yee, B. A.; Zhou, B.; Louie, A. L.; Aigner, S.; Fu, X. D.; Lécuyer, E.; Burge, C. B.; Graveley, B. R.; Yeo, G. W. A Large-Scale Binding and Functional Map of Human RNA-Binding Proteins. *Nature* **2020**, *583*, 711−719.
(40) Klaeger, S.; Gohlke, B.; Perrin, J.; Gupta, V.; Heinzlmeir, S.; Helm, D.; Qiao, H.; Bergamini, G.; Handa, H.; Savitski, M. M.; Bantscheff, M.; Médard, G.; Preissner, R.; Kuster, B. Chemical Proteomics Reveals Ferrochelatase as a Common Off-Target of Kinase Inhibitors. *ACS Chem. Biol.* **2016**, *11*, 1245−1254.
(41) Lechner, S.; Malgapo, M. I. P.; Grätz, C.; Steimbach, R. R.; Baron, A.; Rüther, P.; Nadal, S.; Stumpf, C.; Loos, C.; Ku, X.; Prokofeva, P.; Lautenbacher, L.; Heimburg, T.; Würf, V.; Meng, C.; Wilhelm, M.; Sippl, W.; Kleigrewe, K.; Pauling, J. K.; Kramer, K.; Miller, A. K.; Pfaffl, M. W.; Linder, M. E.; Kuster, B.; Médard, G. Target Deconvolution of HDAC Pharmacopoeia Reveals MBLAC2 as Common Off-Target. *Nat. Chem. Biol.* **2022**, 1−9.

https://doi.org/10.1021/acschembio.2c00500
ACS Chem. Biol. 2022, 17, 3100−3109